Triangular Spectral Element Methods
for Geophysical Fluid Dynamics Applications

B.A. Wingate[*]   J.P. Boyd[†]

Abstract

This work discusses spectral element methods in R^2 on triangular subdomains for application to problems in geophysical fluid dynamics. Methods using triangles as their subdomains are of interest because it is easier to break irregularly shaped domains into triangles than the more commonly used rectangular subdomains. Dubiner has derived a basis which is optimal for many engineering applications where diffusion plays an important role. His 'modified' basis gives sparse matrices for both the weight matrix and the Laplacian operator, making it ideal for semi-implicit schemes which treat diffusion implicitly and advection explicitly. Large scale geophysical fluid dynamic simulations have different requirements than for engineering applications; methods optimal for one class of problems are not necessarily optimal for the other. This work uses a different basis set, an '*interior-orthogonal*' basis, which retains the most important properties of his 'modified' basis, but gives a weight matrix which is simpler.

Key words: triangles, spectral element, geophysical fluid dynamics.

AMS subject classifications: 42C05, 65P05, 86A05.

1   Introduction

There are two main reasons why spectral element techniques have been used recently for geophysical fluid dynamics (GFD) applications. First, spectral elements have

[*]Department of Atmostpheric, Oceanic and Space Science, University of Michigan, and Sandia National Laboratories, 2455 Hayward Avenue, Ann Arbor, MI 48109 (wingate@engin.umich.edu)

[†]Department of Atmostpheric, Oceanic and Space Science and Laboratory for Scientific Computation, University of Michigan, 2455 Hayward Avenue, Ann Arbor, MI 48109 (jpboyd@engin.umich.edu)
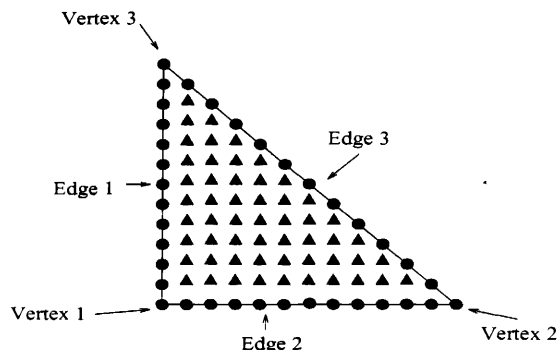
Figure 1: Mode numbers on the reference triangle.

stronger geometric flexibility than spectral methods that use a single expansion for the entire globe. Second, spectral elements are much easier to implement on today's generation of supercomputers, massively parallel architectures, than their globally spectral counterparts.

Geometric flexibility is especially important in GFD. Even in the most complex engineering application, such as a jet engine with moving parts, the length scale of the geometry usually remains fixed and is relatively smooth since it has been manufactured by humans. In contrast, an ocean basin has a fractal boundary. The coast twists and turns on multiple length scales from the width of a continent to the lee of a breakwater. Indeed, each grid refinement in an ocean basin leads to a longer perimeter and can give significantly different boundary-element orientations. While there are no horizontal boundaries in the atmosphere, the bottom topography is as irregular and multi-scaled as a sea bottom. This type of geometry is difficult to represent with rectangular subdomains and can lead to skewed rectangles with non-uniform spatial resolution. This is a strong motivation for exploring spectral elements whose subdomains are triangles.

In addition to the convenience and ease with which domains can be triangulated using unstructured gridding techniques, it is well known in the finite element commu-
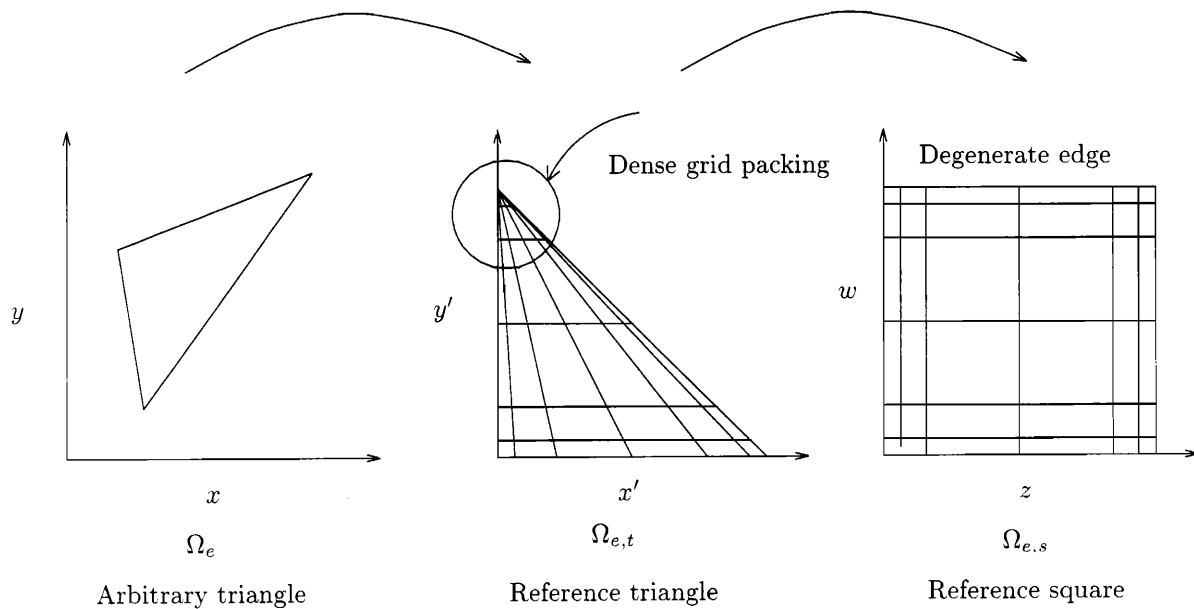
Figure 2: Spatial mappings

nity that the stability of numerical schemes on quadrilaterals degenerates as the vertex angles become more acute. It has been shown that triangles, however, do not have this problem. Triangles whose angles approach zero can still give a convergent algorithm (see, for example, Babuška and Aziz [1]).

Previous work with spectral element methods in GFD and other branches of fluid dynamics typically used quadrilateral subdomains. This allows the use of a tensor product basis so that grid-to-spectral transforms can be calculated by partial summation [2] at a cost of only $O(N^3)$ operations. This technique is crucial to having an efficient numerical algorithm in multi-dimensional problems. A non-tensor product basis, as usually employed with triangular finite elements, has a cost proportional to $O(N^4)$ which is an order of magnitude higher. Also, at higher order the finite element non-tensor product basis becomes dependent and ill-conditioned.

One approach for using higher-order polynomials on triangles is to map each triangle of the physical domain into a square in the computational domain. There are two difficulties with this method. The first problem is that mappings from a triangle (with three corners) to a square (with four corners) map one corner into two. This implies these mappings will introduce non-physical singularities into the problem which interfere with achieving the exponential convergence rates of the high order polynomi-

als. The second problem is that by mapping one corner into two there will be dense grid packing in one corner of the physical domain, see Figure 2. This excessively small grid size severely limits the maximum time step via the CFL condition.

Drawing on ideas from Orszag's [3] important work in spherical harmonics, Dubiner [4] has overcome these difficulties. Dubiner's basis is well suited for solving the Navier Stokes equations for moderate Reynolds numbers where the time step is limited by diffusion. His method gives a sparse element matrix for both the weight matrix and the Laplacian operator. This is optimal for the implementation of a semi-implicit scheme (where the advective terms are treated explicitly and the diffusion terms are treated implicitly).

The physics of fluid dynamics on planetary scales can be very different from mechanical and aeronautical applications which are often dominated by acoustic waves and/or diffusion processes. The Reynolds number for most GFD application is very large ($\sim 10^8$), so the solution is principally driven by advection. Dissipation in large scale GFD models is usually employed to control computational noise rather than to represent physical dissipation which is much smaller. Filtering or a damping proportional to the biharmonic operator is often used in place of the usual viscosity proportional to the Laplacian operator. Also, as the grid size is reduced, dissipation is reduced making the

CFL limit for diffusion as large or larger than the limit for advection so there is little advantage to treating the diffusion terms implicitly. Most oceanographic spectral element models (e.g. Ma [5], Iskandarani [6]) are explicit in contrast to the semi-implicit methods usually employed by engineers.

For these reasons, Dubiner's 'modified basis', which was designed to calculate the Laplacian operator implicitly at every time step, is not optimal for many large scale fluid problems. A better method for geophysical calculations is to exploit the orthogonality of the basis as much as possible, making the structure of the weight matrix more sparse, and thus making the calculation cheaper. To that end, this paper discusses alternatives.

In section (2) we will discuss Dubiner's 'modified' basis and how to manipulate it and give a sample formulation for the heat equation. Section (3) presents several versions of an 'interior-orthogonal' basis and discusses its advantages and disadvantages. Finally, section (4), contains some remarks.b

2 Dubiner's basis

In this section, we discuss Dubiner's 'modified' basis, explain why it is successful for approximating solutions to time-dependent partial-differential equations, and give a brief example of its implementation. In Dubiner's paper, he discusses the implementation of this basis, but a more thorough discussion along with applications to the incompressible Navier-Stokes equations is given by Sherwin and Karniadakis [7]. The basis is broken up into interior modes, edge modes, and vertex modes as shown in Figure 1. This boundary-conscious basis allows for a reasonable means of coupling the elements together while still enforcing C^0 continuity along the boundaries.

We first note that there are two mappings involved in using this basis. The first mapping is from any arbitrarily oriented triangle to a reference triangle. The second is from the reference triangle to a reference square. The second mapping is shown in Figure 2 and is:

$$(1) \qquad x = -1 + \frac{(1-w)(1+z)}{2},$$

and

$$(2) \qquad y = w.$$

The spectral series is given as

$$(3) \qquad u(w,z) = \sum_{m,n \in \overset{1-2}{M}} a_{mn} \overset{1-2}{g}_{mn},$$

where

$$(4) \qquad \overset{1-2}{M} = \{(m,n) | 0 \le m, n; m \le N, m+n \le N\},$$

Interior:

$$(5) \qquad \overset{1-2}{g}_{mn} = (\frac{1+z}{2})(\frac{1-z}{2})\psi^{1,1}_{m-1}(z)$$
$$(\frac{1-w}{2})^{(m+1)}(\frac{1+w}{2})\psi^{2m+1,1}_{n-1}(w),$$
$$m \ge 1, n \ge 1,$$

Edge 1:

$$(6) \qquad \overset{1-2}{g}_{0n} = (\frac{1-z}{2})$$
$$(\frac{1-w}{2})(\frac{1+w}{2})\psi^{1,1}_{n-1}(w),$$
$$n \ge 1,$$

Edge 2:

$$(7) \qquad \overset{1-2}{g}_{m0} = (\frac{1+z}{2})(\frac{1-z}{2})\psi^{1,1}_{m-1}(z)$$
$$(\frac{1-w}{2})^{(m+1)}(\frac{1+w}{2}),$$
$$m \ge 1,$$

Edge 3:

$$(8) \qquad \overset{1-2}{g}_{mN-m} = (\frac{1+z}{2})$$
$$(\frac{1-w}{2})(\frac{1+w}{2})\psi^{1,1}_{n-1}(w),$$
$$m \ge 1,$$

Vertex 1:
$$(9) \qquad \overset{1-2}{g}_{00} = (\frac{1-z}{2})(\frac{1-w}{2}),$$

Vertex 2:
$$(10) \qquad \overset{1-2}{g}_{N0} = (\frac{1+z}{2})(\frac{1-w}{2}),$$

Vertex 3 (corresponds to the degenerate edge):

$$(11) \qquad \overset{1-2}{g}_{0N} = (\frac{1+w}{2}).$$

Here, the $\psi^{\alpha,\beta}_n(x)$ is a Jacobi polynomial defined with the inner product

$$(12) \qquad \int_{-1}^{1} (1-x)^\alpha (1+x)^\beta \psi^{\alpha,\beta}_m(x) \psi^{\alpha,\beta}_n(x) dx.$$

Next we briefly discuss a few of the important properties of this basis.

2.1 Forward/backward transform

We define the backward transform as the transform through which the value of the function at each grid point (quadrature point) is obtained when the spectral coefficients are known. We give the transforms in the mapped (square) domain.

$$(13) \qquad u(w_i, z_j) = \sum_{m,n \in \overset{1-2}{M}} a_{mn} \overset{1-2}{g}_{mn}(w_i, z_j),$$

where $i, j \in \overset{1-2}{K}$, and the space $\overset{1-2}{K}$ is

$$(14) \qquad \overset{1-2}{K} = \{(i,j) | 0 \le i \le K, 0 \le j \le K\}.$$

This sum can be computed in $O(N^3)$ operations using the partial summation technique since the basis is a tensor product. The function along each edge can be computed independent of the interior basis since the interior basis is zero along each boundary.

We define the forward transform as the transform which gives the spectral coefficients when the solution at each quadrature point is known. The grid points are chosen to be the Gaussian quadrature points (see the next section). The forward transformation is obtained by taking the inner product with respect to each side of Equation (13).

$$\int_{-1}^{1} \int_{-1}^{1} u(w, z) \overset{1-2}{g}_{m'n'} \left(\frac{1-w}{2}\right) dw\, dz =$$
$$(15) \quad \sum_{mn} \int_{-1}^{1} \int_{-1}^{1} a_{mn} \overset{1-2}{g}_{m'n'} \overset{1-2}{g}_{mn} \left(\frac{1-w}{2}\right) dw\, dz$$

The factor of $\left(\frac{1-w}{2}\right)$ is a result of the mapping from the triangle to the square. The integrals are evaluated using Gaussian quadrature as discussed in the following section.

2.2 Warped product and Gaussian integration

The integrals in Equation (15) can be broken into the product of two line integrals. Dubiner refers to this property as a 'warped product'. This reduces the cost of computing the area integrals from $O(N_i^2)$ to $O(2N_i)$ where N_i is the order of the quadrature. For an accurate calculation of the integrals, the order of the integration needs to be greater than the maximum degree of the polynomial in $\overset{1-2}{g}_{mn}(w, z)$, denoted by N.

$$\int_{-1}^{1} \int_{-1}^{1} u(w, z) \overset{1-2}{g}_{m'n'}(w, z)\left(\frac{1-w}{2}\right) dw\, dz \quad =$$

$$(16) \qquad \sum_{mn} a_{mn}\left[\int_{-1}^{1} \overset{1}{g}_m(z)\overset{1}{g}_{m'}(z)dz\right]$$
$$\cdot\left[\int_{-1}^{1} \overset{2}{g}_{mn}(w)\overset{2}{g}_{m'n'}(w)\left(\frac{1-w}{2}\right)dw\right]$$

with

$$\int_{-1}^{1} \overset{1}{g}_m(z)\overset{1}{g}_{m'}(z)dz = \sum_{l=0}^{Ni} \overset{1}{g}_m(z_l)\overset{1}{g}_{m'}(z_l)\omega_l^{0,0}$$

$$\int_{-1}^{1} \overset{2}{g}_{mn}(w)\overset{2}{g}_{m'n'}(w)dw = \sum_{l=0}^{Ni} \overset{2}{g}_{mn}(w_l)\overset{2}{g}_{m'n'}(w_l)\omega_l^{1,0}$$

The weight factor is included in the quadrature: $\omega_j^{0,0}$ are the weights for the standard Legendre polynomials using a Lobatto grid and $\omega_j^{1,0}$ are the weights for the $\alpha = 1, \beta = 0$ Jacobi integration on a Lobatto grid.

We point out that there are roughly twice as many quadrature points as basis functions. This can be thought of as using a triangular truncation for the series while employing a square mesh to perform the integration.

2.3 Non-linearity and differentiation

For non-linear terms it is standard practice to transform to physical space to compute the derivatives. From the discussion in the previous section this would appear to be a computationally intensive operation. However, Dubiner points out that in physical space, you are in the same space that is spanned by the Lagrange polynomials (typically used for spectral element methods on rectangular domains) of the same order which can be computed very rapidly, $O(N)$ per differentiation per point. The Jacobi-Lagrange polynomials, also called Cardinal functions, on a Lobatto grid are defined as

$$(17) \qquad C_j^{\alpha\beta}(x) = \frac{(1-x^2)(\psi_N^{\alpha\beta})'(x)}{[(1-x_j^2)(\psi_N^{\alpha\beta})'x_j]'(x-x_j)}$$

where the $\prime$ indicates differentiation. Taken at the Lobatto roots the derivatives have the following analytic form where $\gamma = \alpha + \beta$:

$$\frac{\partial C_j^{\alpha\beta}(x_l)}{\partial x} = \quad -\frac{1}{2} - \frac{n(n+\gamma+1)-(\gamma+2)}{2\beta+4} \quad l = j = 0$$
$$= \quad \frac{1}{2} - \frac{n(n+\gamma+1)-(\gamma+2)}{\beta-\alpha-(\gamma+4)} \quad l = j = N$$
$$= \quad \frac{\mathcal{F}(x_l)}{\mathcal{F}(x_j)(x_l-x_j)} \quad i \ne j$$
$$= \quad -2x_j(\psi_N^{\alpha\beta})''(x_j) + (1-x_j^2)\mathcal{G}(i,j) \quad i = j$$
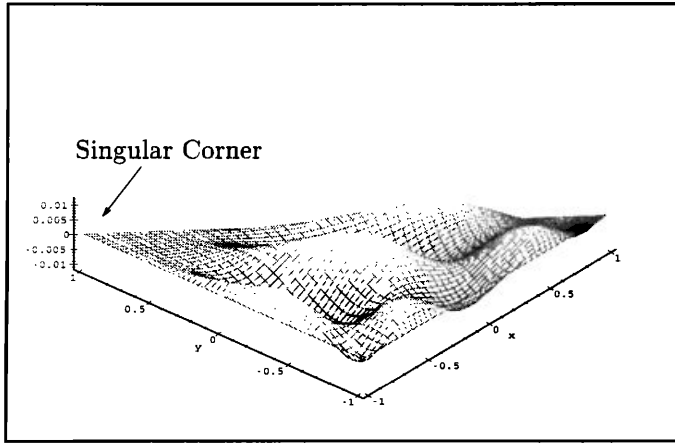
Figure 3: Basis function for m=6,n=2

where

$$\mathcal{F}(x) = \beta - \alpha - \gamma x(\psi_N^{\alpha\beta})'(x) + (n(n+\gamma+1))\psi_N^{\alpha\beta}(x)$$

and

$$\mathcal{G}(i.j) = (\psi_N^{\alpha\beta})'''(x_j) - (\psi_N^{\alpha\beta})''(x_j) \sum_{i=1,i\neq j}^{N-1} \frac{1}{(x_j - x_i)}.$$

Then, for example, the derivative can be computed by

$$(18) \qquad \frac{\partial u}{\partial w}(z_k, w_l) = \sum_{j=0}^{N_i} u(z_k, w_l) \frac{\partial C_j^{1,0}(w_l)}{\partial w}.$$

2.4 Spatial resolution

As mentioned previously, this basis uses a triangular truncation in the modes but requires a square grid of points to perform the quadrature. This means there is dense grid packing in the 'singular' corner. One might think the error would be nonuniform across each triangle, with a higher spatial resolution in this corner, but this is not the case. Therefore, our time step is not limited by the excessive grid spacing in the densely packed corner.

The reason this basis does not over-resolve the singular corner is the $(1 - w)^m$ factor in $\overset{2}{g}_{mn}(w)$. This factor is a function of two parameters: the vertical coordinate, w and the mode number of the horizontal direction. This means as the wave number, m, increases, the factor $(1 - w)^m$ decreases and thus acts like a scaling variable to reduce the amplitude of the w basis. Figure 3 shows the (6,2) basis function. The amplitude and variability of the basis is not large along the degenerate edge (near $w = 1$).

2.5 Boundary coupling

Each side is represented by a Jacobi polynomial, $\psi_n^{1,1}$, which has been carefully devised so that it is zero at all vertices and on the two other sides. The interior modes are also zero on the boundary of the reference triangle. This makes for a relatively straight forward coupling between the elements. We use the word 'relatively' because depending on which sides are abutting, some of the modes of one side may actually be opposite in sign to the modes of its adjacent side.

2.6 Example

As an example of how to formulate problems using this basis, consider the heat equation,

$$(19) \qquad \frac{\partial u}{\partial t} = \frac{\partial^2 u}{\partial x^2} + \frac{\partial^2 u}{\partial y^2},$$

with the initial condition,

$$(20) \qquad u(x,y) = \sin(\pi x)$$
$$\text{for} \quad -1 \leq x \leq 1, -1 \leq y \leq 1,$$

and time varying boundary conditions,

$$u(x,y) = e^{-2t}\sin(\pi x) \quad \text{on} \quad y = -1 \text{ and } y = 1$$
$$u(x,y) = 0 \quad \text{on} \quad x = -1 \text{ and } x = 1.$$

We assume our domain is Ω with P subdomains.

$$(21) \qquad \cup_{e=1}^P \Omega_e = \Omega$$

with the requirement (to couple the boundaries) that

$$(22) \qquad \Omega_i \cap \Omega_j = \partial\Omega_{i,j}$$

where Ω_i and Ω_j are connected and $\Omega_{i,j}$ is their common boundary.

We take the inner product of both sides of Equation (19) and apply the divergence theorem (formally) to obtain the weak form,

$$(23) \qquad \int_\Omega \frac{\partial u}{\partial t}\bar{u}\,d\Omega = -\int_\Omega \frac{\partial u}{\partial x}\frac{\partial \bar{u}}{\partial x} + \frac{\partial u}{\partial y}\frac{\partial \bar{u}}{\partial y}\,d\Omega,$$

Here, the overbar indicates the function is a test function.

Note the boundary terms are zero along the outer boundary and the contribution along element faces cancel because the outward unit normals of abutting triangles are equal and opposite.

With 3rd-order Adams-Bashforth time integration we have,
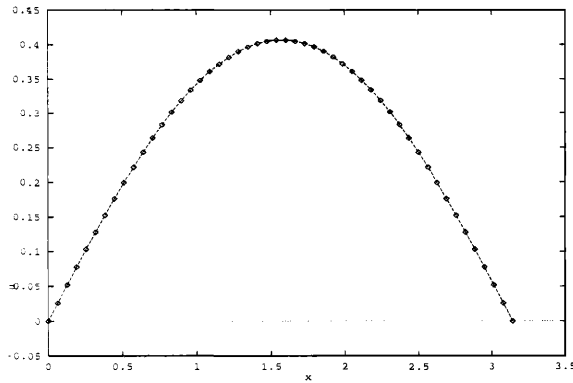
Figure 4: A one dimentional slice of the solution at $y = 0$ compared with the exact solution, $e^{-t}\sin(\pi x)$, at $t = .9$

$$(24) \quad \int_\Omega \frac{u^{n+1} - u^n}{\Delta t} \bar{u} d\Omega =$$
$$- \int_\Omega \sum_{q=0}^{3} \alpha_p \left(\frac{\partial u^{n-p}}{\partial x} \frac{\partial \bar{u}}{\partial x} + \frac{\partial u^{n-p}}{\partial y} \frac{\partial \bar{u}}{\partial y} \right) d\Omega$$

where

$$(25) \quad \alpha_0 = \frac{23}{12},$$

$$(26) \quad \alpha_1 = -\frac{16}{12},$$

$$(27) \quad \alpha_2 = \frac{5}{12}.$$

On every subdomain Ω_e we employ Dubiner's basis set. The formulation can be written as,

$$\sum_{e=1}^{P}{}' \sum_{m'n'} \sum_{mn} \{a_{mn}^{n+1} - a_{mn}^n\} W^e(m', n', m, n) =$$
$$(28) \quad \sum_{e=1}^{P}{}' \sum_{m'n'} \sum_{q=0}^{3} \alpha_p \{a_{mn}^{n-p} R^e(m', n')\}$$

where W^e is the weight matrix,

$$(29) \quad W^e = \sum_{mn} [\sum_{k=0}^{N_i} {}^1g_{m'}(z_k) {}^1g_m(z_k) \omega_k^{0,0}]$$
$$\cdot [\sum_{l=0}^{N_i} {}^2g_{m'n'}(w_l) {}^1g_{mn}(w_l) \omega_l^{1,0}],$$

and $R^e(m', n')$ is a combination of warped product integrals and metric coefficients from the mappings.

Figure 4 shows a one-dimensional slice of the solution for $y = 0$ and $x = -1$ to 1 at $t = .9$ for two triangles. The solution is identical for any arrangement of the triangles.

See Wingate [8] for the details of applying this method for geophysical fluid dynamics simulations.

3 Dubiner's interior - orthogonal basis.

In this section we discuss a different basis set, an 'interior-orthogonal' basis. The interior modes are orthogonal to each other, unlike the 'modified' basis where they are semi-orthogonal. This 'interior-orthogonal' basis can be classified in a similar way to the 'modified' basis.

Interior:

$$(30) \quad {}^{1-2}g_{mn} = (\frac{1+z}{2})(\frac{1-z}{2})\psi_{(m+1)}^{2,2}(z)$$
$$(\frac{1-w}{2})^m (\frac{1+w}{2})\psi_{n-1}^{2m+3,2}(w),$$
$$m \geq 1, n \geq 1$$

Edge 1:

$$(31) \quad {}^{1-2}g_{0n} = (\frac{1-z}{2})$$
$$(\frac{1-w}{2})(\frac{1+w}{2})\psi_{n-1}^{2,2}(w),$$
$$n \geq 1$$

Edge 2:

$$(32) \quad {}^{1-2}g_{m0} = (\frac{1+z}{2})(\frac{1-z}{2})\psi_{m-1}^{2,2}(z)$$
$$(\frac{1-w}{2})^{(m+1)}](\frac{1+w}{2}),$$
$$m \geq 1$$

Edge 3:

$$(33) \quad {}^{1-2}g_{mN-m} = (\frac{1+z}{2})$$
$$(\frac{1-w}{2})(\frac{1+w}{2})\psi_{n-1}^{2,2}(w),$$
$$m \geq 2$$

Vertex 1:

$$(34) \quad {}^{1-2}g_{00} = (\frac{1-z}{2})(\frac{1-w}{2}),$$

Vertex 2:

$$(35) \quad {}^{1-2}g_{N0} = (\frac{1+z}{2})(\frac{1-w}{2}),$$

Vertex 3:

$$(36) \quad {}^{1-2}g_{0N} = (\frac{1+w}{2}).$$

This basis has a weight matrix that looks like Figure (5). It is diagonal and has two boundary bands along the top and left side. The border exists because the boundary bases are not orthogonal to themselves or the interior modes. However, this system has a simpler structure than
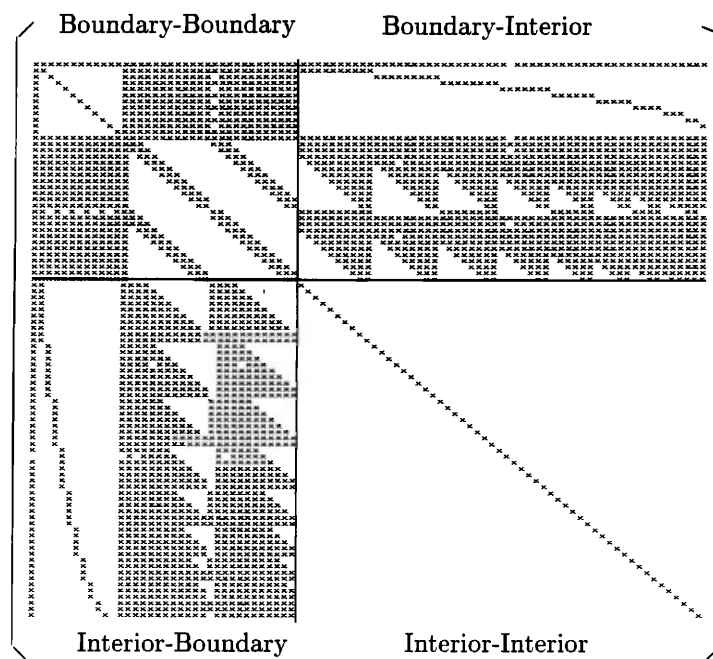
Figure 5: Weight matrix for the 'interior-orthogonal' basis using $\psi_n^{2,2}$ edge functions.

the 'modified' basis whose weight matrix is shown in Figure (6).

Additional sparseness is rendered by using the $\alpha = 1$ and $\beta = 1$ Jacobi polynomials for the edge functions. However, there is still a banded structure of bandwidth $O(3N - 1)$. See Figure (7).

Even more sparseness can be obtained by using the $\alpha = 3$ and $\beta = 2$ Jacobi polynomial (see Figure (8)), but this is a bad choice, since the boundaries cannot be coupled as easily due to the non-symmetric nature of the $\psi_n^{3,2}$ Jacobi polynomial.

The benefit of using the 'interior-orthogonal' basis over the modified basis is twofold.

- Storage: you need only save half of the upper square matrix and one of the boundary bands (since it is a symmetric matrix) and you only need to store the diagonal elements in the lower right hand block. The storage is higher for the modified basis because the diagonal bandwidth is wider (and depends on the maximum degree of the polynomials).

- *LU* factorization: it is very simple to rewrite standard LU decomposition routines to take advantage of the diagonal part of matrix. The cost of inverting the lower square matrix is only $O(N)$. Sherwin

uses the static condensation technique which costs $O(kN^3)$. With the 'interior-orthogonal' basis, the cost is $O(kN^2)$.

NOTE: For $N \geq 4$ the 'interior-orthogonl' basis always gives part of the stiffness matrix to be diagonal. The 'modified' basis will give a full matrix for low degrees of N.

NOTE: The first item, above, also applies to the global stiffness matrix. If the stiffness matrix is assembled by cycling through the boundaries and vertices before the interior modes, the structure of the global matrix will be similar to the form in Figure 5.

The disadvantages are

- For both the 'modified' and the 'interior-orthogonal' basis the weight matrix must be stored (less for the 'interior-orthogonal' basis). This is a disadvantage when compared to the spectral element method on rectangles where the weight matrix does not need to be stored.

- The 'interior-orthogonal' method gives a full element matrix for the Laplacian operator.
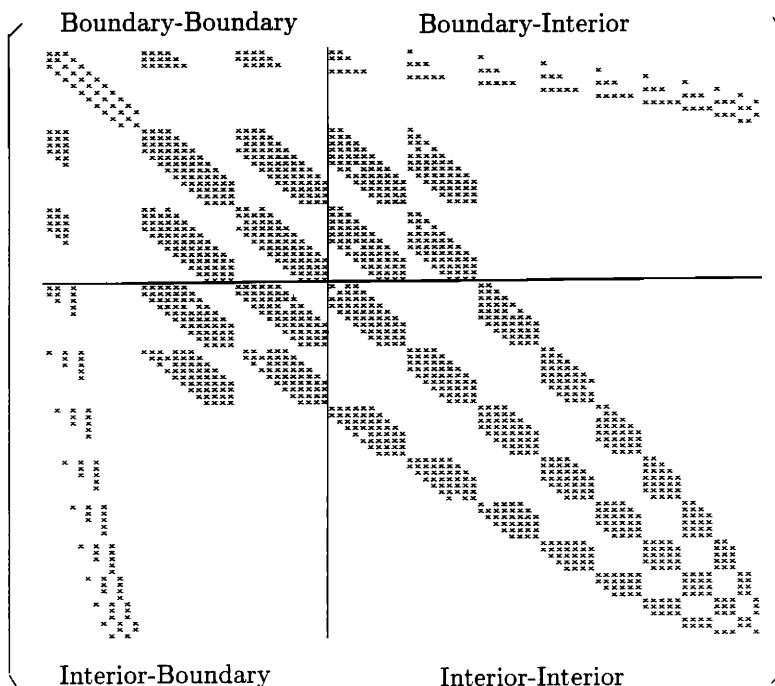
Figure 6: Weight matrix for Dubiner's modified basis.
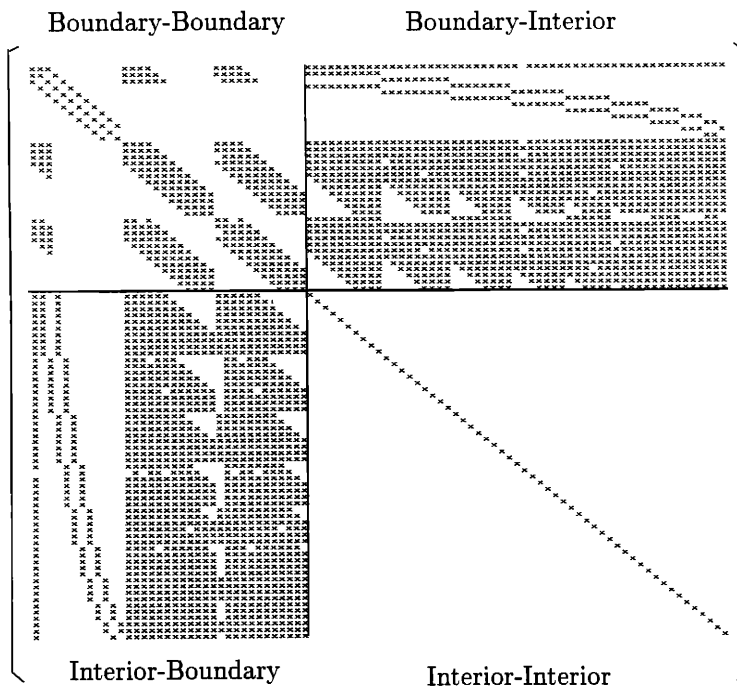
Figure 7: Weight matrix for the 'interior-orthogonal' basis using $\psi_n^{1,1}$ edge functions.

Boundary-Boundary   Boundary-Interior

Interior-Boundary   Interior-Interior
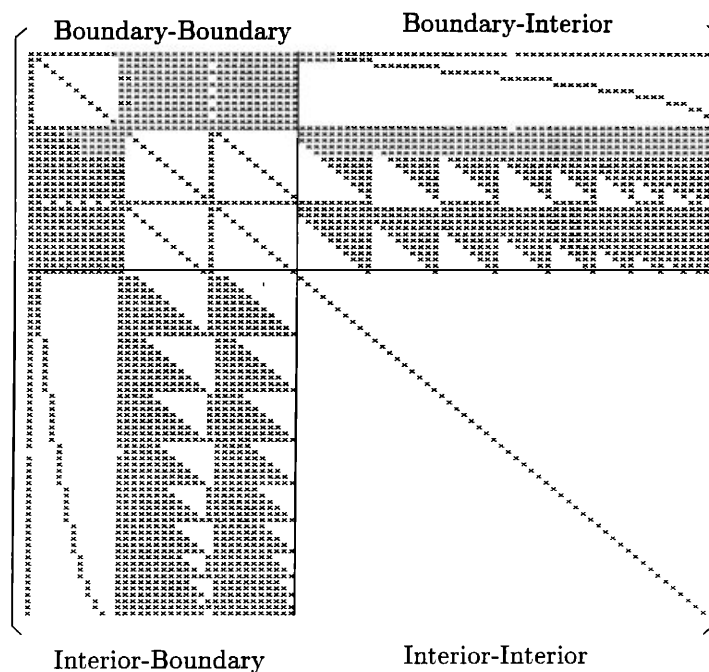
Figure 8: Weight matrix for the 'interior-orthogonal' basis using $\psi_n^{3,2}$ edge functions.

4 Conclusions

We have given an 'interior-orthogonal' alternative to Dubiner's originally posed 'modified' basis. Our motivation for using the 'interior-orthogonal' basis is that we are able to exploit more of the orthogonality between the modes, leading to a system of equations which is cheaper to solve for explicit methods. For large scale GFD applications, explicit methods are more efficient for the time discretization. There are three advantages to the 'interior-orthogonal' basis as follows: 1) For the interior-interior part of the weight matrix you need only store the diagonal elements and 2) a fast LU factorization which takes advantage of the diagonal part of the weight matrix is *simple* to implement. Dubiner's 'modified' basis is optimal for problems which have processes in which diffusion plays a role equally as important as advection. For this type of process, the 'interior-orthogonal' basis would give a full matrix for the Laplacian operator which would be a disadvantage.

In summary, we are motivated to use triangular subdomains because of the geometric complexity of our boundaries (in GFD and other branches of fluid dynamics). While it is very cheap to use explicit methods on rectangular domains (one need not even store the weight matrix), near these complicated boundaries rectangular elements are highly skewed; triangular elements allow a more uniform discretization which permits the use of a higher time step. Looked at that way, the cost per element per time step is actually cheaper.

5 Acknowledgments

References

[1] I. Babuška and A. Aziz, "On the angle condition in the finite element method," *SIAM Journal of Numerical Analysis*, vol. 13, 1976.

[2] S. Orszag, "Spectral methods for problems in complex geometries," *J. of Comp. Phys.*, vol. 37, pp. 70–92, 1980.

[3] S. Orszag, "Fourier series on spheres," *Mon. Wea. Rev.*, vol. 102, pp. 56–75, 1973.

[4] M. Dubiner, "Spectral methods on triangles and other domains," *J. Sci. Comp.*, vol. 6, pp. 345–390, 1993.

[5] H. Ma, "A spectral element basin model for the shallow water equations," *J. of Comp. Phys.*, vol. 109, pp. 133–149, 1993.

[6] M.Iskandarani, D.Haidvogel, and J.P.Boyd, "A staggered spectral finite element method for the shallow water equations," *To appear: Int. J. Num. Meth. Fl.*, 1994.

[7] S. Sherwin and G. Karniadakis, "A triangular spectral element method; applications to the incompressible navier-stokes equations," *To appear: Comp. Meth. Appl. Mech. and Engr.*, 1995.

[8] B.A.Wingate, *Spectral Elements using Triangular Subdomains for Geophysical Fluid Dynamics Applications.* PhD thesis, University of Michigan, 1996.